Pentacene ultrathin film formation on reduced and oxidized Si surfaces

Ricardo Ruiz,[1] Bert Nickel,[2,3] Norbert Koch,[3,4] Leonard C. Feldman,[1] Richard F. Haglund,[1] Antoine Kahn,[3,4] and Giacinto Scoles[2,3]

[1]*Vanderbilt University, Department of Physics and Astronomy, Nashville, Tennessee, 37235*

[2]*Princeton University, Chemistry Department, Princeton, New Jersey, 08544*

[3]*Princeton Materials Institute, Princeton, New Jersey, 08544*

[4]*Princeton University, Department of Electrical Engineering, Princeton, New Jersey, 08544*

(Received 3 September 2002; published 12 March 2003)

We have compared the nucleation of pentacene on reduced and oxidized Si surfaces by a combination of x-ray reflectivity measurements and atomic force microscopy. For the reduced surface, the nucleation density is 0.007 μm^{-2}. Second monolayer (ML) formation starts at a coverage of $\Theta=0.6$ ML, and the first layer is completely closed at a total coverage of 2 ML. For the oxidized surface, the nucleation density is larger by a factor of 100 (0.7 μm^{-2}). Second ML formation also starts at $\Theta=0.6$ ML, but the first layer closes already at 1.1 ML coverage, indicating nearly ideal layer-by-layer growth. For both terminations, the electron density obtained for the closed first monolayer is only 75% of the bulk value, indicating a reduced mass packing efficiency of the layer. Second ML islands are aligned relative to each other on an area limited by the lateral size of first ML islands, which act as templates for epitaxial growth.

DOI: 10.1103/PhysRevB.67.125406 PACS number(s): 68.55.Ac, 61.10.Kw, 61.66.Hq

I. INTRODUCTION

Organic/inorganic interfaces are currently under investigation due to their critical role in molecular and bioelectronic technology.[1–3] Among the various materials being studied, pentacene ($C_{22}H_{14}$), a long, flat, aromatic molecule (see Fig. 1) is particularly promising for electronic applications. Pentacene forms good crystals if deposited onto flat, inert surfaces, resulting in highly anisotropic transport properties.[4] Pentacene is used to fabricate organic thin film transistors (OTFT's) in applications where large area coverage, mechanical flexibility, and room temperature processing are required.[5,6] In such devices, high field-effect mobilities up to 1.5 $cm^2/(V\,s)$[7] have been reported along with a variety of OTFT configurations and designs.[3,8,9]

Charge transport in an OTFT is confined to the first few monolayers in close proximity to the gate oxide (the channel).[10] Extensive work has been devoted to determine and optimize the charge transport properties of mesoscopic pentacene films (thickness range from 10 nm to 1 μm)[11–14] and to relate these properties to the crystalline structure and morphology. However, in order to disentangle structural aspects from fundamental limits of charge transport in organic materials, the confinement of the charge transport towards the gate oxide demands a detailed study of the early stages of film formation since these layers dominate charge transport.

In this paper we report a combined atomic force microscopy (AFM) and synchrotron x-ray reflectivity differential study of pentacene film formation on two different surface terminations [Fig. 1(e,f)] prepared by applying standard wet etching techniques to a thermally oxidized Si wafer. In our analysis, we focus on the coverage and structure of the first few monolayers. Our work is complementary to recent experiments, in which photoelectron emission microscopy (PEEM) demonstrated that pentacene film formation can be improved considerably by making use of a cyclohexane termination of clean Si(001) surfaces[15] or by means of hyperthermal beam-deposition energies.[16] Here, we demonstrate that similar full first layer coverage and layer-by-layer growth may also be achieved for clean oxide and H-terminated Si surfaces. We also demonstrate that different substrate terminations, having dissimilar surface energies, result in completely different morphologies and nucleation densities.

II. EXPERIMENTAL DETAILS

A. Substrate preparation

Since pentacene film formation is controlled by relatively weak van der Waals interactions, nucleation of the first monolayer (ML) is extremely sensitive to defects or impurities on the substrate surface which act as pinning centers. Heterogeneous surfaces lead to a wide range of morphologies and piling up of material, making the interpretation of properties, such as field effect mobility, difficult. To minimize the influence of surface impurities, we have applied the

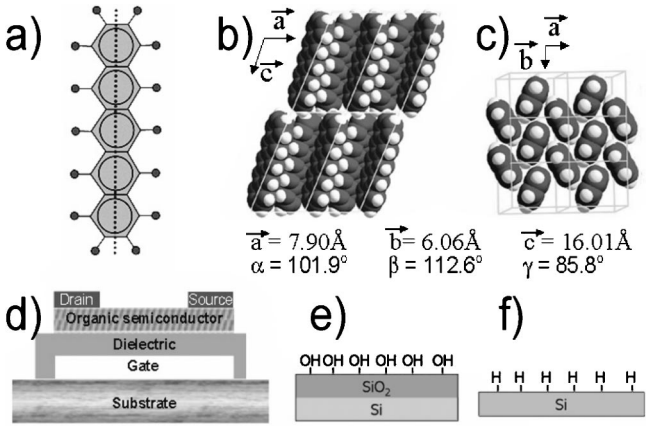

FIG. 1. (a) Molecular structure and (b) and (c) crystalline structure of pentacene. (d) Typical OTFT geometry (top contact), (e) O/OH terminated Silicon oxide, (f) H atom terminated Si.

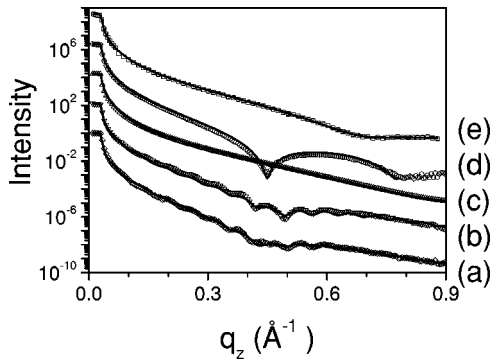

FIG. 2. X-ray reflectivity data of the chemically treated Si wafer. (a) Thermal oxide after cleaning in acetone. (b) Hydrophilic oxide termination obtained by step I. (c) H-termination resulting from step II. (d) Hydrophilic reoxidation layer after step III. (e) Hydrophilic reoxidation layer while keeping the sample at ~350 °C.

following three step wet-etching procedures (highest purity chemicals have been purchased from Aldrich). Substrates were prepared from silicon (100) wafers with 100 Å of thermally grown oxide.

Step I. A clean oxide, hydrophilic termination was obtained by sonication in acetone for 30 min, boiling in acetone, followed by boiling in $H_2O_2(30\%) + H_2SO_4(99.99\%)$ (3:1) for 45 min and rinsing in deionized water (DI water).

Step II. Reduced, hydrophobic, H atom terminated silicon substrates were obtained by etching in a <5% HF solution for 30 s followed by etching in a <1% HF solution for 3 min and rinsing in DI water.[17]

Step III. A chemically reoxidized, hydrophilic surface was obtained by boiling in $HNO_3(70\%)$ for 15 min and followed by rinsing in DI water.

Step I removes organic contamination from the thermal oxide surface. During step II, the thermal oxide is removed, and after rinsing, the surface is reduced by the H atom termination. Step III is intended to chemically reoxidize the topmost Si bilayer in a controlled way.[18]

Sample substrates obtained after each of the steps outlined above plus another substrate only cleaned with boiling acetone (see step I), were placed in a x-ray vacuum chamber ($p = 1\times10^{-7}$ mbar) within less than 10 min after preparation to verify the outcome of the chemical treatment by x-ray reflectivity measurements. The reflectivity data (dots) and least squares simulations (solid lines) are summarized in Fig. 2.

For the acetone cleaned sample, the reflectivity reveals the presence of a 96 Å thick oxide, in good agreement with the specification [Fig. 2(a), see Sec. II C for details about the x-ray reflectivity measurements]. After the surface cleaning (step I), the thickness of thermal oxide is unchanged [Fig. 2(b)]. Furthermore, an additional water layer ($d\sim7$ Å) is adsorbed on the surface, as revealed by a least squares fit [solid curve in Fig. 2(b)]. This water layer manifests itself in the reflectivity data as a dip at $q_z = 0.45$ Å. After etching (step II), a featureless Fresnel-like reflectivity curve is obtained [Fig. 2(c)], indicating that the oxide has been removed successfully. Reoxidation (step III) gives rise to a pronounced dip and bump structure [Fig. 2(d)]. Gentle heating of the sample to ~350 °C removes part of this structure [Fig. 2(e)]. Therefore, it is reasonable to conclude that a water layer is also present after reoxidation. A least square fit analysis of the reoxidized sample before and during heating allows to quantify this conclusion; for the fresh reoxidized sample we find a surface region of 11 Å with decreasing electron density, while for the hot reoxidized sample the extent of this region is only 7 Å. We therefore conclude that the fresh reoxidized surface consists of ~7 Å chemical oxide and a ~4 Å water overlayer.

B. Atomic force microscopy

Films analyzed with AFM (Digital Instruments Nanoscope III SPM) were evaporated in an ultrahigh vacuum chamber. The deposition rate was monitored with a quartz crystal microbalance (QCM) and was kept constant at 1.25×10^{-3} nm/sec (or 1 ML/20 min assuming 1 ML~1.5 nm) for all experiments. The substrate was held at room temperature during deposition. Background pressure during evaporation was 7×10^{-10} Torr. Twelve pentacene films were evaporated on oxidized (step I) and reduced (steps I and II) substrates, respectively. The film thickness ranged from 0.15 to 2.0 ML. After evaporation, the samples were taken to an *ex situ* AFM (soft tapping mode) for characterization. Island nucleation densities and fractional coverage have been determined from images taken at larger scales than shown here (40 μm for the reduced surface and 20 μm for the oxidized one). A surface root mean square (r.m.s.) roughness of 0.17 nm was determined from a standard analysis of AFM scans from bare substrates.

Throughout the text, we express film thicknesses by an equivalent amount of standing, close packed ML's. Furthermore, the pentacene layer in direct contact with the substrate is termed the first layer. Fractional coverage of a layer denotes the percentage of area covered by the deposited material.

C. X-ray reflectivity

X-ray experiments were carried out at the National Synchrotron Light Source (NSLS) at the Exxon beamline X10B. Pentacene films were evaporated *in situ* in a transportable vacuum chamber equipped with a 270° beryllium window, a Knudsen cell, a quartz crystal microbalance (QCM), and a sample holder that allows temperature control from 200 to 500 K. Deposition rate and substrate temperature were the same as for the AFM experiments. Background pressure during evaporation was 1×10^{-7} Torr. Pentacene films were evaporated on H terminated and reoxidized substrates obtained from steps I and II, and I, II, and III, respectively. The time between substrate preparation and evacuation of the sample environment was less than 30 min. Successive x-ray measurements were performed at 0.0, 0.5, 1.0, and 2.0 ML coverage.

Measurements were carried out in reflectivity mode at a wavelength of $\lambda = 0.1123$ nm. In this mode, the scattering vector ($q_z = 4\pi/\lambda \sin\Theta$) is along the surface normal. The

reflected intensities are simulated using a program based on the Parratt formalism.[19] As a result of such analysis, a (laterally averaged) depth resolved electron density profile is obtained. The length scale of the lateral average is given by the lateral coherence length ($\xi_{||}$). Depending on the x-ray optics, $\xi_{||}$ may easily reach several μm at a synchrotron source.[20] From the rocking width of the specular beam, we estimate a value of ($\xi_{||} \sim 2$ μm) for our setup at X10B. The comparison of the as-deduced electron densities with the tabulated values of, e.g., the bulk crystalline phase of pentacene allows for an estimate of the packing density of the deposited films, as well as for a characterization of the substrate surface obtained from the chemical treatment.

III. EXPERIMENTAL RESULTS

A. AFM measurements

Selected AFM micrographs of pentacene films for various film thicknesses ranging from the submonolayer regime up to 2 ML are shown in Fig. 3. Films grown on H terminated and oxidized substrates correspond to the left and right columns, respectively. At a coverage of 0.14 ML, the island density of the H terminated substrate is 0.007 μm^{-2} [Fig. 3(a)], while for the oxidized substrate it is 0.7 μm^{-2} at a similar coverage [Fig. 3(f)]. Thus, a striking difference in the nucleation density depending upon the substrate preparation is revealed. Furthermore, after increasing the film thickness to 0.5 ML, the new material is incorporated into the present nuclei keeping the nucleation density almost constant [Figs. 3(b), 3(g)]. Coalescence of first ML islands starts beyond film thicknesses of 0.5 ML.

On the oxidized substrate, at a coverage of 1.02 ML an almost closed first monolayer is formed [Fig. 3(h)] in coexistence with some second ML nuclei. As coverage is increased, second layer islands grow [Fig. 3(i)] and eventually coalesce [Fig. 3(j)]. After second ML coalescence, the film exhibits some cracklike features [Fig. 3(j)].

On untreated substrates, impurities may act as nucleation centers, favoring the piling up of pentacene molecules and therefore hampering well ordered layer-by-layer growth, as shown by the way of example in the inset in Fig. 3(i).

The island step heights ($\sim$15 Å) observed with AFM give a first estimate of the interplanar spacing. The average value of the step height for the first layer was 16.5$\pm$3 Å for the H-terminated substrate and 13.8$\pm$3 Å for the oxidized Si. Similarly, the average step heights for the second layer (i.e., the step from the first to the second layer) were 13.0$\pm$3 Å and 15.0$\pm$3 Å, respectively. These values are comparable to the molecule length indicating a vertical orientation of the molecules in agreement with the well known thin-film phase in which the plane spacing d_{001} is reported to be 15.4 Å.[14]

On the H terminated substrate, second layer nucleation is observed well before the first layer closes. The fractional coverage of each layer as a function of the total coverage is summarized in Fig. 4. The solid lines indicate the ideal case of layer-by-layer growth in which all of the deposited material initially goes to the first layer and nucleation of the second layer does not take place until first layer completion. The

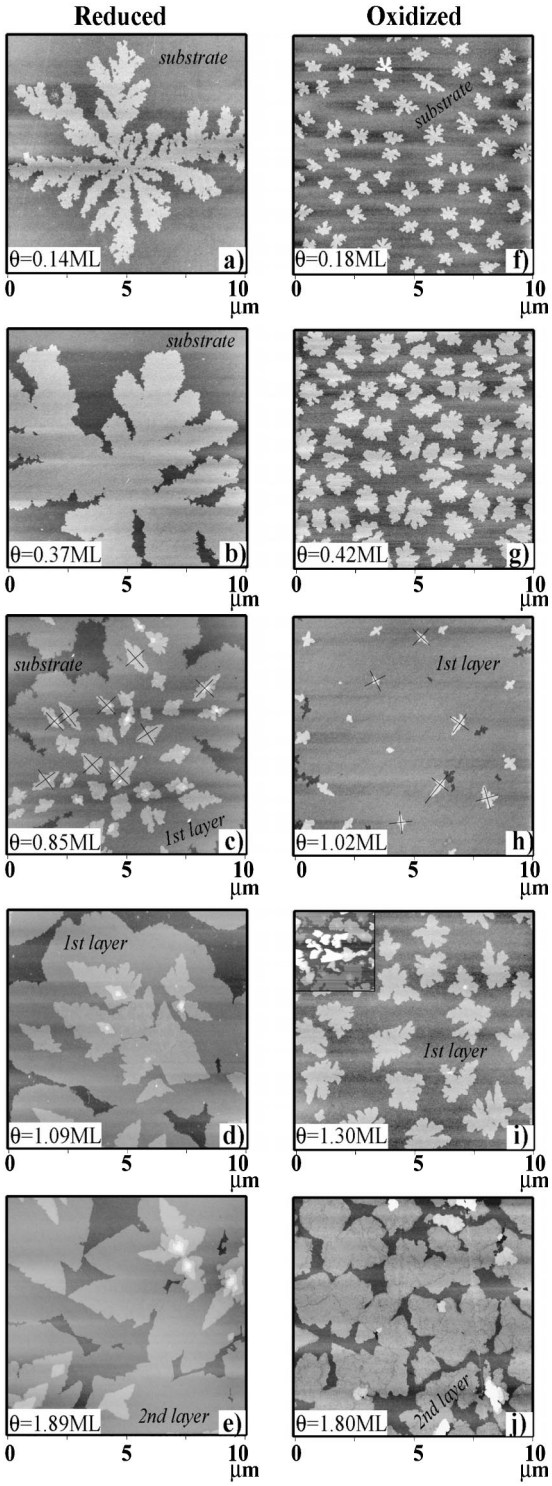

FIG. 3. AFM images of pentacene film formation on H terminated (left column) and oxidized (right column) substrates, with the total film thickness Θ ranging from 0.14 to 1.89 ML, as indicated. The molecular steps associated with the various layers are visible and selected regions have been labeled for clarity (substrate, first layer, second layer). The orientation of faceted second layer islands is indicated by the cross axes [(c) and (h)]. The heterogeneous film structure obtained in presence of surface impurities is also shown for comparison in (i) as an inset (same scale).

vertical dashed lines indicate the actual values at which full coverage of the first layer is achieved.

The fractional coverage curve for the H terminated substrate [Fig. 4(a)] indicates that nucleation of the second and third layers starts when the previous layer reaches about 60% coverage. The first layer is completed at a total coverage of $\theta=2$ ML. This is similar to reports for pentacene films on clean Si substrates.[15]

For the oxidized substrate, a slight onset of second ML nucleation is also observed at $\theta=0.6$ ML but significant condensation of the second ML starts only at $\theta=1.1$ ML, i.e., once the first layer is complete. Thus, comparing the two substrates, only the oxidized substrate favors a closed first ML and nearly ideal layer-by-layer growth without the presence of significant second ML condensation. Figure 4 will be discussed in more detail at the end of the next subsection in direct comparison to x-ray measurements.

B. X-ray measurements

The x-ray reflectivity data obtained for the films deposited onto the H terminated and reoxidized substrates are shown as points in Figs. 5(a) and 5(b), together with the least-square simulations shown as solid lines. The electron densities associated with the simulations are shown in Figs. 5(c) and 5(d). The four data sets for each sample correspond to the bare substrate and to nominal film thickness of 0.5, 1.0, and 2.0 ML, as indicated.

The bare H terminated substrate gives rise to a smooth, featureless intensity distribution which can be readily simulated by the Fresnel reflectivity of a Si crystal exhibiting a surface r.m.s. roughness of $\sigma=0.27$ nm. The fact that the substrate roughness measured by x-ray reflectivity is slightly larger than that measured by AFM can be explained by size effects of the AFM tip (typically 10 nm), which systematically underestimate the peak-to-valley value of the surface corrugation.

After deposition of 0.5 ML pentacene, an eye inspection of the reflectivity data for the H terminated substrate reveals intensity oscillations [Fig. 5(a), Kiessig fringes[21]], indicating the formation of a well-defined layered structure. A rough estimate of the oscillation period ΔQ for the submonolayer regime ($\Delta Q\sim 0.4$ Å^{-1} or $D=2\pi/\Delta Q=16$ Å) indicates the presence of a standing phase of thickness D [Fig. 1(b)]. The approximate value of 16 Å also compares well with the AFM step measurements and with the thin film d_{001} spacing. Increasing the total coverage to 1 ML, the intensity oscillations become more pronounced while the oscillation period ΔQ remains rather unchanged. This indicates that mainly the first monolayer is filled up during deposition. The reflectivity for the 2 ML samples shows a doubling of the oscillation period and a beating effect, which corresponds to a film that is now twice as thick and exhibits a reduced density for the second monolayer. Kiessig fringes have not been reported for pentacene films in the literature so far, indicating the importance of the chemical substrate preparation procedure for a substantial improvement of film morphology.

The reflectivity of the bare reoxidized surface is more pronounced, giving rise to a dip- and bumplike structure

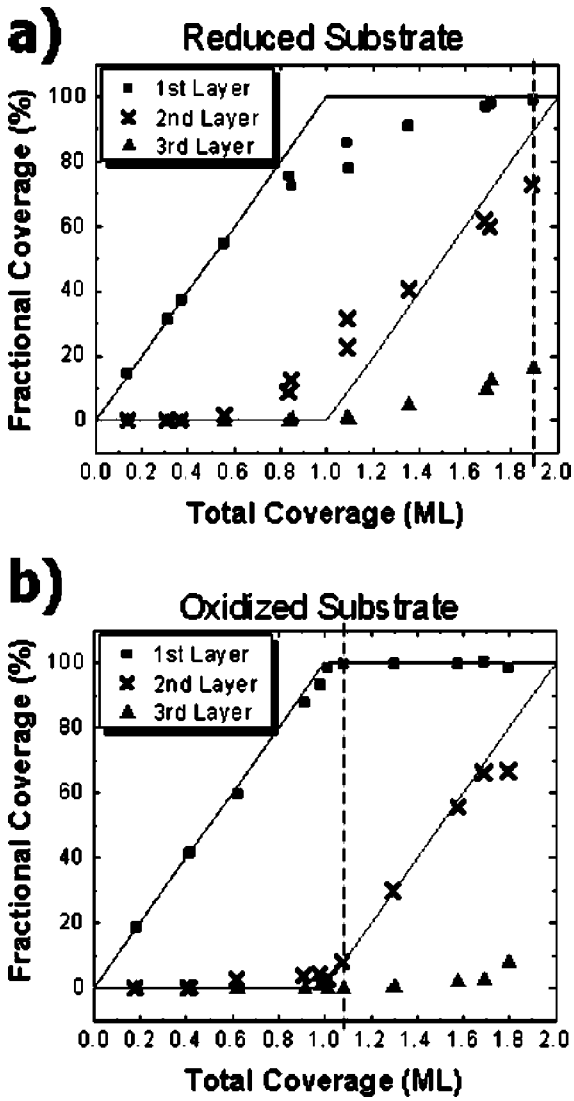

FIG. 4. Fractional coverage for pentacene deposited on H terminated (a) and oxidized (b) Si substrates vs total coverage.

[Fig. 5(b)]. A least-squares fit indicates the presence of a surface region with a thickness of 1.1 nm and a continuously decreasing electron density [see solid line in Fig. 5(d)]. We associate this region with the microscopic reoxidation layer, the OH termination and the water adlayer that follows from step III. A good simulation of the reflectivity data is possible using the Parratt formalism. For convenience, the obtained profiles have been normalized to the electron density of Si [0.70 e/Å^3 (Ref. 22)]. The volume of the bulk pentacene unit cell is 692 Å^3,[23–25] and considering that there are two molecules within the unit cell, and 146 electrons per molecule, then the electron density of bulk pentacene is 0.42 e/Å^3. Thus, the density of bulk pentacene relative to that of Si is 0.60 [vertical dashed line in Figs. 5(c) and 5(d)].

In the following, the profiles [Figs. 5(c) and 5(d)] obtained for the two surface terminations are compared and analyzed. For both terminations, the density of the first layer increases during deposition up to a maximum value of $\sim$0.45; the optimal value of 0.6 is not reached. However, since AFM suggests a tightly closed first layer for a film thickness of 2 ML, the most likely explanation for the ob-

served low density is a less efficient packing. If the bulk phase is regarded as the most efficient packing configuration with a relative density of 0.6, the other extreme of a least efficient packing (with no voids) could be regarded as made out of boxlike molecules. Drawing a rectagular box along the Van der Waals surface of the molecule yields a box of dimensions 16.577, 7.447, and 3.885 Å.[26] That is, a volume per molecule of 479.6 $Å^3$ and thus obtaining an electron density of 0.30 $e/Å^3$ or a density of 0.43 relative to that of Si. The relative density of a full pentacene layer with a nonoptimal packing density should lie somewhere in between 0.43 and 0.6 [i.e., in between the two dashed lines of Figs. 5(c) and 5(d)]. Even though it is well known that the "thin film phase" obtained in evaporated pentacene thin films differs from the bulk phase,[14] a full characterization of the unit cell is not available yet so as to calculate the relative density of the thin film phase.

Considering that there is a closed first layer, we take the relative density of 0.45 obtained from the x-ray simulations to define a full ML. Based on this assumption, the fractional coverage of the first monolayer will be estimated and discussed now. After deposition of 0.5 ML of pentacene, both substrates show the formation of a standing phase of similar density ($\rho/\rho_{Si}=0.2$). This value, compared to the maximum values of 0.45, indicates a fractional coverage of the first layer of 0.2/0.45=44% for both substrates, in reasonable agreement with the AFM analysis [Figs. 4(a) and 4(b)], which also revealed no difference in fractional coverage at this stage.

At a film thickness of 1 ML, the first monolayer densities differ. In turn, the fractional coverage of first monolayer on the reoxidized surface is (0.38/0.45=84%), while for the H terminated substrate it is only (0.3/0.45=67%). This trend of faster closing of the first layer for the oxidized substrate is again in good agreement with the AFM observation.

Finally, at a film thickness of 2 ML, the fractional coverage of the second layer on the H terminated substrate is (0.27/0.45=60%), in reasonable agreement with the AFM measurement. For the reoxidized substrate, however, the fractional coverage of the second layer is (0.14/0.45=31%) only. This is considerably less than the respective value obtained from the AFM measurement (70%). The deviation may partly result from a variation in the deposition rate, which, however was checked regularly during deposition. Also, the quality of the fit is worst for the 2 ML sample, indicating that eventually the description of the sample by a well-defined layered structure is no longer fully appropriate.

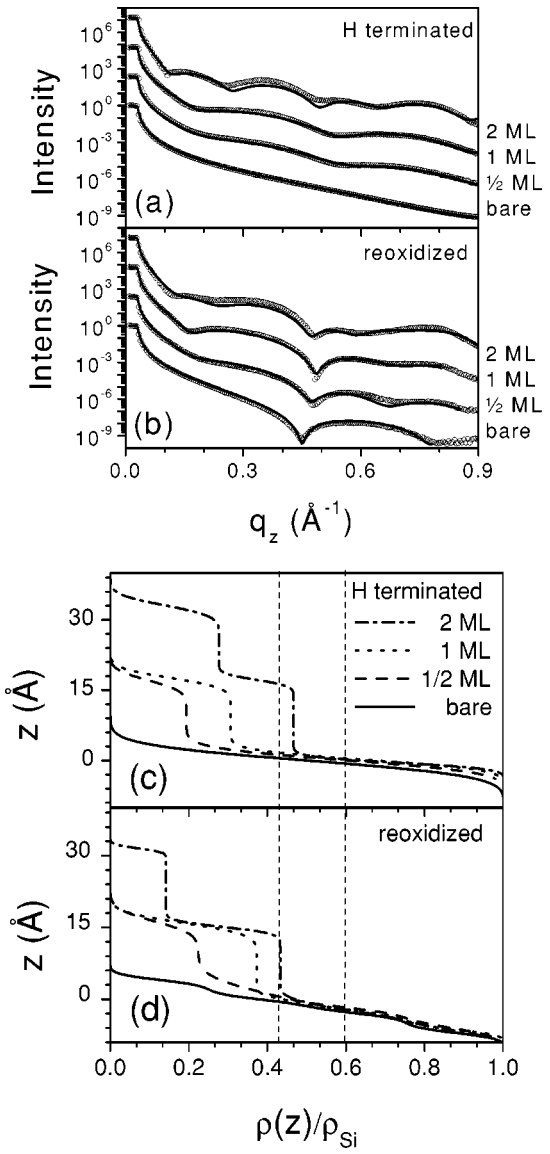

FIG. 5. X-ray reflectivity. (a), (b) Reflectivity data for a nominal film thickness of 0, 0.5, 1, and 2 ML pentacene on a H terminated and reoxidized surface, respectively. (c), (d) Normalized electron density profiles [$\rho(z)/\rho_{Si}$] obtained from the least-squares analysis [solid lines in (a), (b)]. The vertical dashed lines indicate the density of bulk-crystalline pentacene [$\rho(z)/\rho_{Si}=0.6$] and the density of a boxlike molecule [$\rho(z)/\rho_{Si}=0.43$].

IV. DISCUSSION

A. Submonolayer regime

For the deposition of pentacene on reduced (H terminated) and oxidized substrates, respectively, a two orders of magnitude difference in nucleation density (0.007 μm^{-2} vs 0.7 μm^{-2}) has been observed. The microscopic mechanism which provoke this rather different growth behavior will be discussed now.

The fractal shape of the islands on the reduced substrate at low coverage [Fig. 3(a)] resembles the morphology predicted by diffusion limited aggregation theory (DLA),[27,28] as expected for systems incorporating deposition, diffusion and aggregation (DDA) in the submonolayer regime.[29,30]

For the oxidized substrate a strong increase of the nucleation density is observed. While the possible influence of localized pinning centers of unknown origin can not be excluded, the kind of impurities that cause piling up of pentacene aggregates [inset of Fig. 3(i)] are clearly absent in the chemically treated substrates. We therefore conclude that the difference in nucleation and packing of the first pentacene ML on the two surface terminations results from a hindered surface diffusion of the pentacene molecules on the oxidized substrate rather than the presence of isolated pinning centers.

Further work to quantify the surface diffusion parameters is in progress.

B. Complete first monolayer

On the H-terminated substrate pentacene forms a complete full first layer only when the total deposited material reaches almost 2 ML as indicated by the dashed lines in Fig. 5. On the oxidized sample, pentacene completes a closed first layer already when the total deposited material adds up to 1.1 ML. Apparently, pentacene completes the first ML faster on the oxidized substrate because of its larger nucleation density. The microscopic mechanism that explains these findings can be sketched as follows. When a molecule lands on an island, it diffuses until it finds another molecule to form a new immobile cluster or, if it does not find a second molecule, it will continue diffusing till it encounters a step edge. If a step edge represents an extra potential-energy barrier (Schwoebel barrier[31]) then the molecule will stay on top of the island resulting in a three-dimensional (3D) growth mode. But if the energy barrier is absent or at least well below the thermal energy of the molecule, then the molecule will hop off the island to the lower layer.

Schwoebel barriers may not be present in pentacene growth since second layer nucleation does not occur till the total coverage reaches about 60%, and second layer nucleation does not happen on step edges either, as confirmed with AFM. Due to the smaller island size in the oxidized substrates as compared to the reduced ones, once a pentacene molecule is deposited on a first-layer island on an oxidized surface, it has a large probability to diffuse along the island and make it down a step-edge before finding another molecule. Thus, the larger nucleation density and the absence of a significant Schwoebel barrier are causing a faster completion of the first layer in oxidized substrates. However, the larger island density that is contributing to a faster closing of the first-layer is also increasing the concentration of grain boundaries once the first-layer islands coalesce since the first-layer islands are not oriented with respect to one another.

On H-terminated substrates there may not be Schwoebel barriers either, since there is no second-layer nucleation on step edges and there is no 3D growth. However, since the average island size is much larger than its oxidized counterpart, it becomes much more likely for a molecule diffusing on such a large first-layer island to find other molecules starting a second layer nucleation well before finding a step edge. On the other hand, since the first-layer islands are much larger in this substrates, the result is a much lower concentration of grain boundaries once the first layer is completed.

C. Second monolayer

The low nucleation density observed for the first layer on reduced substrates does not apply for the nucleation of pentacene on pentacene (i.e., the second ML on the first ML). However, second layer islands apparently keep the crystal orientation of the island below them. The morphology of the second layer for both substrates is characterized by islands having a rhomboid shape with two perpendicular axes [Figs. 3(c) and 3(h)]. We associate these axes with the herringbone structure characteristic for pentacene crystals [Fig. 1(c)] and its polymorphs.

On the reduced substrates, the nucleation density of the second-layer islands is higher than the one on the first layer. Having a larger number of islands on the second layer implies that a number of those would nucleate on top of a single first layer island. If they all mimic the crystal structure of the underlying island, the result would be a group of second-layer islands that have an identical alignment as long as they rest on the same first-layer island. This alignment can indeed be observed on the second-layer islands of Fig. 3(c) indicating also that even though the packing density is not optimal, there is still crystal structure. When such an aligned group of second-layer islands coalesce, the concentration of grain boundaries would be minimal resulting in local epitaxy limited only by the size of the first-layer island.

For the oxidized sample, the nucleation density of the second-layer islands is comparable (even slightly lower) to that of the first layer. In this case, on average, there would be one second-layer island per first-layer island, or in some cases there would be a single second-layer island on top of more than one islands. Assuming that all first-layer islands have random orientations, and considering that the second layer islands would copy the crystal structure of the island underneath, then all second layer islands would have random orientations as well [Fig. 3(h)]. Eventually, when these islands grow and coalesce, they will introduce a high concentration of grain boundaries that could also lead to some stress within the same layer islands. In a similar way, second layer islands that lie on top of more than one first-layer islands would face a certain lattice mismatch due to the different alignments of the islands underneath inducing some interplanar stress. Attempts to address the detailed molecular arrangement at the grain boundaries from diffuse x-ray intensities are currently in progress. In this context, it is also important to note that not only the grain boundaries may have a negative impact on the electronic properties of pentacene, but also the nonoptimal packing density observed with the x rays may pose intrinsic limits to the field effect mobility.

Our results explain a previous transmission electron micrograph study which indicated that pentacene films optimized for OTFT applications are composed of grains with a typical lateral size of 400 nm, which are aligned with each other over distances of 3 μm .[32] We suggest that the alignment is due to the first monolayer, which can act as a template for epitaxial growth. Since the grain boundary concentration can reduce the field effect mobility in an OTFT,[33] the outlined mechanism is important to understand the limitations encountered in the various OTFT configurations.

V. CONCLUSIONS

The chemical treatment of Si-wafer surfaces in order to obtain oxidized and reduced surfaces promotes homogeneous nucleation and growth that is governed by surface diffusion rather than by impurities, roughness or other inhomogenities. AFM images confirmed the formation of a

closed first layer. X-ray reflectivity indicates that the density of this layer is only 75% of what would be expected from a bulk-like closely packed layer. Faster closing of the first layer occurs for the oxidized substrate, but at the expense of a higher nucleation density leading in turn to smaller island sizes and a higher concentration of grain boundaries. In conclusion, the morphology of the first layer is strongly influenced by the surface termination. In a later stage of the growth process, when pentacene nucleates on pentacene, the morphology of the first layer turns out to be crucial in determining the outcome of subsequent layers as the latter grow epitaxialy on top of the first layer islands. This suggests that the grain size in mesoscopic pentacene film is mostly limited by the lateral size of the initial ML islands. We have demonstrated that a reduced surface termination is most promising for growing larger single crystal films.

ACKNOWLEDGMENTS

We thank the NSLS management and the beamline staff and scientists from Exxon (S. Bennett and R. Kolb) for continuous support and M. Shtein, L. Casalis and M. F. Danisman for valuable discussions and great help. The work at Princeton and at the NSLS has been supported by the DOE under Grant No. DE-FG02-93ER45503. R.R. acknowledges the support of a Vanderbilt University Discovery Grant. BN acknowledges financial support from the Deutsche Forschungsgemeinschaft (Grant No. DFG Ni1-1).

[1] C. D. Dimitrakopoulos, S. Purushothaman, J. Kymissis, A. Callegari, and J. M. Shaw, Science **283**, 822 (1999).
[2] D. Gundlach, L. Zhou, J. Nichols, J.-R. Huang, C. Sheraw, and T. Jackson, in *Electron Devices Meeting, 2001, IEDM Technical Digest, International* (Penn State University Press, University Park, PA, 2001).
[3] C. Kim, M. Shtein, and S. R. Forrest, Appl. Phys. Lett. **80**, 4051 (2002).
[4] T. Minakata, H. Imani, M. Ozaki, and K. Saco, J. Appl. Phys. **72**, 5220 (1992).
[5] D. Knipp, R. A. Street, B. Krusor, R. Apte, and J. Ho, J. Non-Cryst. Solids **299-302**, 1042 (2002).
[6] C. Sheraw, L. Zhou, J.-R. Huang, D. Gundlach, T. Jackson, M. G. Kane, I. G. Hill, M. S. Hammond, J. Campi, and B. K. Greening, Appl. Phys. Lett. **80**, 1088 (2002).
[7] Y.-Y. Lin, D. Gundlach, S. Nelson, and T. Jackson, IEEE Electron Device Lett. **18**, 606 (1997).
[8] D. J. Gundlach, L. L. Jia, and T. N. Jackson, IEEE Electron Device Lett. **22**, 571 (2001).
[9] D. Gundlach, Y. Lin, T. Jackson, S. Nelson, and D. Schlom, IEEE Electron Device Lett. **18**, 87 (1997).
[10] A. Dodabalapur, L. Torsi, and H. E. Katz, Science **268**, 270 (1995).
[11] M. L. Swiggers, G. Xia, J. D. Slinker, A. A. Gorodetsky, and G. G. Malliaras, Appl. Phys. Lett. **79**, 1300 (2001).
[12] H. Klauk and T. Jackson, Solid State Technol. **43**, 63 (2000).
[13] M. Kasaya, H. Tabata, and T. Kawai, Surf. Sci. **400**, 367 (1998).
[14] C. D. Dimitrakopoulos, A. R. Brown, and A. Pomp, J. Appl. Phys. **80**, 2501 (1996).
[15] F.-J. Meyer Zu Heringdorf , M. C. Reuter, and R. M. Tromp, Nature (London) **412**, 517 (2001).
[16] L. Casalis, M. F. Danisman, B. Nickel, G. Bracco, T. Toccoli, S. Iannotta, and G. Scoles (unpublished).
[17] K. Endo, K. Arima, K. Hirose, T. Kataoka, and Y. Mori, J. Appl. Phys. **91**, 4065 (2002).
[18] U. Neuwald, A. Feltz, U. Memmert, and R. J. Behm, J. Appl. Phys. **78**, 4131 (1995).
[19] L. G. Parrat, Phys. Rev. **95**, 359 (1954).
[20] H. Dosch, *Critical Phenomena at Surfaces and Interfaces: Evanescent X-ray and Neutron Scattering*, Vol. 126 of Springer Tracts in Modern Physics (Springer, Berlin, 1992).
[21] H. Kiessig, Ann. Phys. (N.Y.) **5**, 769 (1931).
[22] W. G. Wyckoff, *Crystal Structures*, 2nd ed. (Krieger, Dordrecht, 1981), Vol. 1.
[23] J. M. Robertson, V. C. Sinclair, and J. Trotter, Acta Crystallogr. **14**, 697 (1961).
[24] R. B. Campbell, J. M. Robertson, and J. Trotter, Acta Crystallogr. **14**, 705 (1961).
[25] R. B. Campbell and J. M. Robertson, Acta Crystallogr. **15**, 289 (1961).
[26] L. C. Sander and S. A. Wise (unpublished).
[27] T. A. Witten, Jr. and L. M. Sander, Phys. Rev. Lett. **47**, 1400 (1981).
[28] P. Meakin, Phys. Rev. A **27**, 1495 (1983).
[29] P. Jensen, A.-L. Barabási, H. Larralde, S. Havlin, and H. E. Stanley, Phys. Rev. E **50**, 618 (1994).
[30] A.-L. Barabási and H. E. Stanley, in *Fractal Concepts in Surface Growth* (Cambridge University Press, Cambridge, 1995), pp. 175–191.
[31] R. L. Schwoebel and E. J. Shipsey, J. Appl. Phys. **37**, 3682 (1966).
[32] J. G. Laquindanum, H. E. Katz, A. J. Lovinger, and A. Dodabalapur, Chem. Mater. **8**, 2542 (1996).
[33] G. Horowitz and M. E. Hajlaoui, Synth. Met. **122**, 185 (2001).